BMC Cardiovascular Disorders

RESEARCH

Open Access

Construction of AMPK-related circRNA network in mouse myocardial ischemia–reperfusion injury model

Yang Song[1], Yi Zhao[1], Xiaodi Zhang[1], Cheng Cheng[1], Haidong Yan[1], Daxing Liu[1] and Dengshen Zhang[1*]

Abstract

Objective To screen Myocardial ischemia–reperfusion Injury in mice. adenosine monophate-activatedprotein kinase (AMPK) -related differentially expressed circularRNA (circRNA) in MIRI model, Ampk-related circRNA network was drawn to provide possible ideas for the prevention and treatment of MIRI.

Methods The mouse MIRI model was constructed by ligation of the left anterior descending artery. After the model was successfully established, the related indicators of cardiac function were detected, and high-throughput sequencing was performed on the myocardial tissue of the mice.

Results MIRI model was successfully constructed, and two AMPK related differentially expressed loops (novel_circ_043550 and novel_circ_035243) were screened out. A circRNA-miRNA-mRNA network consisting of 2 circRNA, 28 microRNA(miRNA) and 229 messengerRNA (mRNA) was constructed.

Conclusions This study reveals the differential expression of several AMPK-related circRNAs in MIRI in mice, and the AMPK-related circRNA regulatory network is constructed, suggesting that AMPK-related circRNA may have potential clinical application prospects as a potential molecular marker and therapeutic target for MIRI.

Keywords circRNA, MIRI, RNA-seq, ceRNA, AMPK, Bioinformatics

Myocardial ischemia–reperfusion Injury (MIRI) refers to the interruption of myocardial blood supply for a short period of time, and the restoration of blood supply for a certain period of time, the original ischemic myocardium occurs more serious damage than ischemia [1]. It is the main cause of cardiac dysfunction and even death after coronary thrombolysis, coronary interventional surgery and Cardiopulmonary bypass (CPB) open heart surgery [2, 3]. Reducing or eliminating such damage is one of the urgent problems in the cardiovascular field. Previous studies have shown that mitochondrial dysfunction causes accumulation of reactive oxygen species (ROS) and dysfunction of adenosine triphosphate (ATP) synthesis in cells. It is one of the important mechanisms of MIRI [4, 5]. AMP-activated protein kinase (AMPK) is a heterotrimeric protein composed of α, β and γ subunits [6, 7], which is a member of the serine/threonine protein kinase family. It can be activated under conditions such as ischemia, hypoxia, fasting, and exercise. Activated AMPK can sense changes in the energy metabolism of cells, participate in a variety of metabolic processes in cells, and is a sensor to maintain intracellular energy balance [8]. AMPK is widely present in eukaryotic cells. By promoting myocardial mitochondrial biosynthesis [9], inhibiting excessive fission of myocardial mitochondria [10] and maintaining the activity of myocardial mitochondrial autophagy, it achieves endogenous myocardial

*Correspondence:
Dengshen Zhang
xwkzds2021@163.com
[1] Department of Cardiovascular Surgery, Affiliated Hospital of Zunyi Medical University, Zunyi, Guizhou 563000, China

protective effect [11, 12], and maintains the dynamic balance of myocardial mitochondrial function through the regulation of mitochondrial function by cohesion. It can inhibit the abnormal accumulation of ROS and promote the production of mitochondrial ATP, so as to play an anti-MIRI effect [13].

The current drugs and strategies for the prevention and treatment of MIRI still do not achieve very ideal results in clinical practice, and there may be other unrecognized or valued factors involved. For example, circleRNA (circRNA) and other previously neglected non-coding RNA(ncRNA) play an urgent role in MIRI, which needs to be further explored [5]. circRNA is a special class of non-coding RNA molecules. End to end connected to form a closed ring, which is not easily degraded by RNA enzymes, is considered to be a potential biomarker [14]. circRNA plays a regulatory role at the transcriptional and post-transcriptional levels, and is involved in various cardiovascular physiological and pathological processes such as embryogenesis, cardiovascular development, heart failure, myocardial hypertrophy, myocardial fibrosis, and myocardial apoptosis. Recent studies have shown that some circRNA in myocardial tissue cells are involved in the regulation of mitochondrial function and play an important role in the mechanism of MIRI [15]. Given that AMPK is an important molecule regulating mitochondrial function [16], these circRNA molecules related to mitochondrial function show the regulatory effect of myocardial MIRI. It may be closely related to AMPK. In order to further clarify the mechanism of MIRI, we screened AMPK-related differentially expressed circRNA in MIRI, constructed AMPK-related circRNA regulatory network, speculated and explored the molecular mechanism of MIRI, and provided possible research basis for finding potential circRNA diagnostic markers of MIRI. As shown in the Fig. 1.

Materials and methods

Experimental animals

Male C57BL/6 mice, 6–8 weeks old, weighing 18–24 g, 32 in total. They were purchased from Guizhou HuiJiu Biotechnology Co., Ltd. and fed in the animal room of the Public Laboratory Center for Clinical Medicine of the Affiliated Hospital of Zunyi Medical University, with the room temperature of 22–26℃, humidity of 45–55%, ventilation, and regular illumination around the clock, and the mice were free to drink and eat. This experiment has been approved by the Experimental Animal Ethics Committee of the Affiliated Hospital of Zunyi Medical University (Ethics number: zyfy-an-2023–0221).

Experimental grouping and MIRI model construction

Thirty-two male C57BL/6 mice were randomly divided into four groups: Sham group ($n=8$), MIRI group ($n=8$), MIRI + AMPK agonist adipocarcin (5-Aminoimidazole-4-carboxamide1-β-D-ribofuranoside,AICAR) ($n=8$), and MIRI + AMPK inhibitor Dorsomorphin (Compound C) group ($n=8$). The mouse MIRI model was constructed

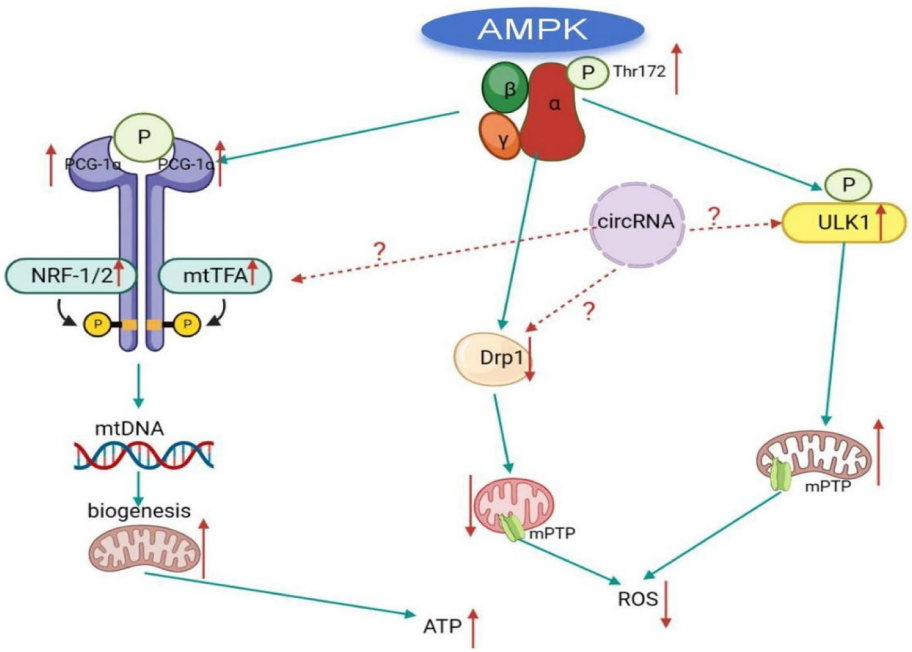

Fig.1 Key molecules and regulatory networks that mediate cardiac mitochondrial function after AMPK activation

by ligating the left anterior descending artery [17, 18]. Each mouse was anesthetized with a concentration of 3% pentobarbital (0.75 ml/kg), and the skin was prepared, disinfected, and a sterile towel was spread after the anesthesia was effective. The subcutaneous and pectoralis major tissues were separated layer by layer to expose the intercostal space. The 3–4 intercostal space was used as the surgical entry port. The bending forceps were used to gently press the intercostal space with a sense of loss. The color of the heart tip changed from red to white, and the ECG showed ST segment elevation. Then the heart was put back into the chest and the wound was closed tightly. At the same time, excess blood gas was quickly removed. To achieve the purpose of myocardial ischemia–reperfusion [19]. As shown in Fig. 2.

Sham group did not do any treatment, MIRI group did not do any drug intervention, MIRI + AICAR group and MIRI + Compound C group were given corresponding drugs by intraperitoneal injection 1 h before operation. The doses of AICAR solution and Compound C solution were 100 mg/kg and 10 mg/kg, respectively [20]. Except Sham group, myocardial reperfusion was achieved by ligating the left anterior descending artery and removing the coronary ligating line 30 min later in the other three groups, so as to construct MIRI model. After natural recovery, the heart tissues of the mice were collected for detection of cardiac related indicators after 1 week of feeding. High-throughput sequencing technology and bioinformatics technology were used to capture differentially expressed circRNA. Cluster software was used to screen differentially expressed circRNA molecules coexisting in the ischemia–reperfusion myocardium for cluster analysis, and GO function and KEGG pathway analysis of differentially expressed circRNA genes were performed. Ampk-related circRNA molecules closely related to MIRI were mined, and the accuracy of the screening results was verified by real-time fluorescent quantitative polymerase chain reaction (qRT-PCR). Finally, the candidate circRNA molecules were screened, and the expression profile of AMPK-related circRNA was drawn.

Identification of differentially expressed AMPK-related circRNAs

In this study, RNA extraction and high-throughput sequencing of myocardial tissue samples were commissioned by Shenzhen BGI Technology Service Co., LTD.

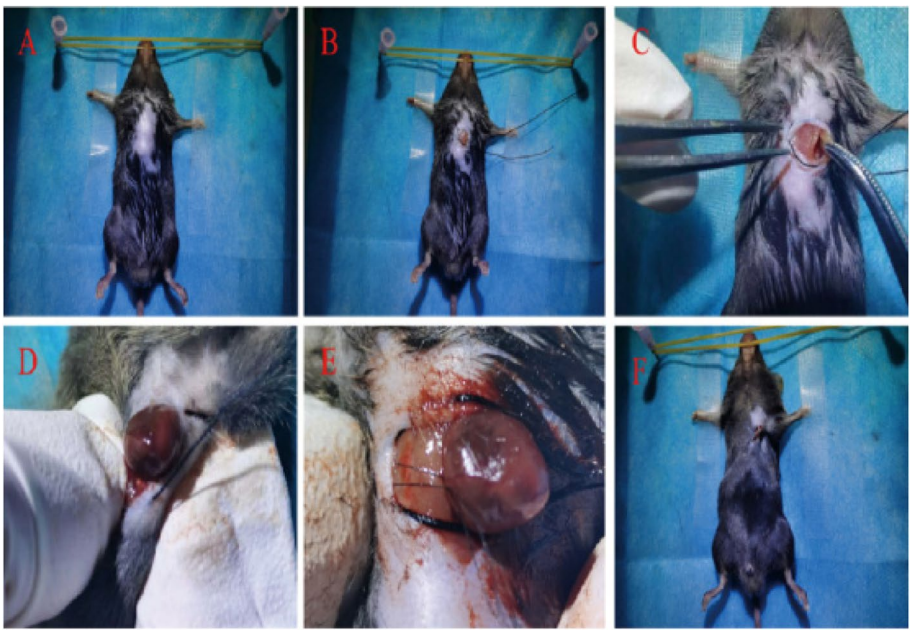

Fig.2 Establishment of mouse MIRI model (A: anesthesia, disinfection, fixation. B: make a 1 cm incision 0.5 cm outside the left sternum of the mouse, and use 3–0 silk thread to close the purse-string suture. C: separate the subcutaneous tissues and the pectoralis major muscle tissues layer by layer, and expose the intercostal space, use the 3rd ~ 4th intercostal space as the surgical access, and use curved forceps to press gently and feel the sensation of falling out. D: the left thumb with the forefinger to press on the incision, making the heart "pop out". D: The left thumb and index finger apply pressure on the incision to make the heart "pop out". E: A 7–0 wire was used to ligate near the root of the aorta and 1 mm below the left auricle, and the color of the heart tip was observed to change from red to white. F: The heart was retracted into the chest cavity, and the incision was closed.)

Data analysis process

The raw data generated by sequencing were called raw reads, firstly, we filtered out the reads with low quality, connector contamination and high content of unknown base N, and the filtered data were called clean reads, and then the clean reads were compared to the reference genome, and the circRNAs were predicted by the two software programs, CIRI and find_circ, and the results of the two software programs were merged. After combining the results of the two software, the genes from which the circRNAs originated were annotated in Gene Ontology (GO) and Kyoto Encyclopedia of Genes and Genomes (KEGG) databases, and the genes from which the circRNAs originated were analyzed by quantitative and differential expression analysis, and the genes from which the differential circRNAs originated were enriched by GO function. The circRNAs were quantified and differentially expressed, and the genes with different circRNA origins were analyzed for GO functional enrichment and Pathway functional enrichment. Finally, the genes of circRNA origin were analyzed for miRNA target gene prediction in this study [21]. The complete analysis flow is shown in Fig. 3.

CircRNA prediction and annotation

CircRNAs were predicted using two software programs, CIRI [22] and find_circ [23], and the results of the two software programs were integrated based on the start and end positions of circRNAs [24].CIRI was based on the genome matching algorithm of BWA-MEM [25], and it detects circRNAs through the Sequence Alignment Map (SAM) file generated from two scans matching. CIRI is based on the BWA-MEM genome alignment algorithm, and detects circRNAs by comparing the SAM (Sequence Alignment Map) files generated from two scans. the front and back parts of the same read need to be cross-referenced to the genome in order to prove that they are junction reads of circRNAs. Therefore, during the first scanning process, CIRI will filter the junction reads with Paired Chiastic Clipping (PCC) signals, and then further filter the junction reads by the restriction of Paired-end Mapping (PEM) range and GT-AG clipping signals. junction reads are further filtered. In the second scanning of the SAM file, CIRI detects new junction reads and also excludes false-positive circRNAs caused by incorrect matching to homologous genes or repetitive sequences, thus improving the sensitivity and accuracy of the software. The specific process was shown in Fig. 4A. find_circ was a software based on Bowtie2 [26, 27] to compare genomes. First, find_circ discards the reads that can be aligned to the genome in a continuous and full-length manner, and then extracts 20 bp from the ends of the remaining reads to align the genome, and those sequences that can be cross-referenced to the exons can be used to prove the existence of circRNAs. This part of the aligned sequences will be extended to collect further information about the junction site. Finally, candidate circRNAs are obtained through a series of filtering strategies. The specific process was shown in Fig. 4B.

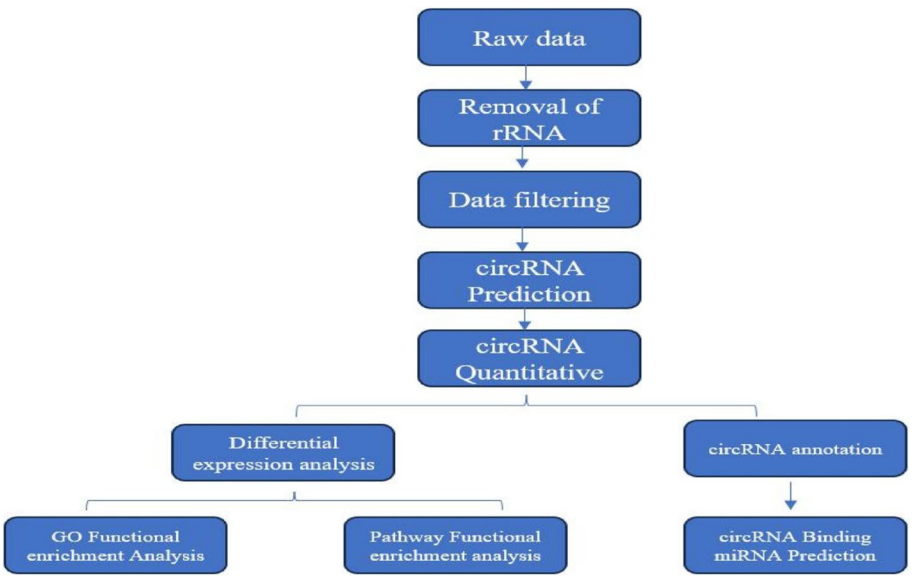

Fig.3 Flowchart of circRNA information analysis

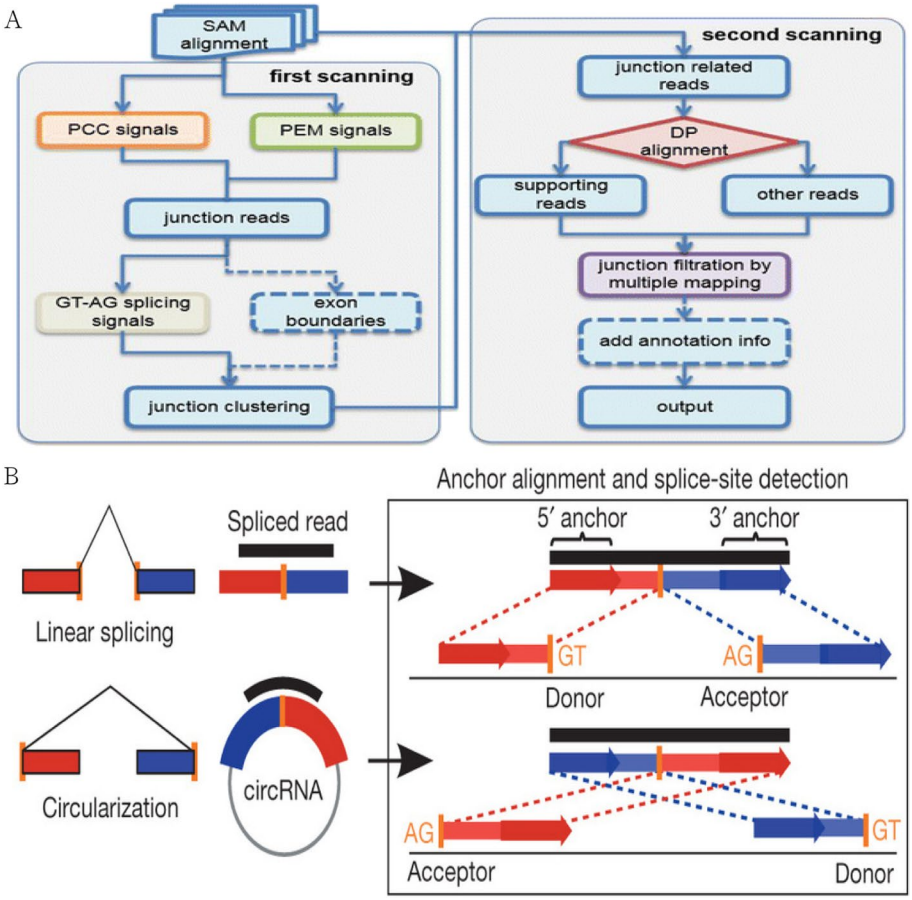

Fig.4 (A: Flowchart of circRNA detection by CIRI, B: Schematic diagram of find_circ for detecting circRNA)

Screening of differential circRNAs

In this study, we used the differentiallye xpressed genes from RNA-seq data (DEGseq) algorithm [28] for the detection of differentially circRNAs.According to the amount of gene expression, genes with differences in gene expression levels in each group are called differentially expressed genes (differentially expressed gene,DEG), RNA sequencing can be treated as a random sampling process, where each read is taken independently and uniformly from the sample. Under this assumption, the number of reads from a gene follows a binomial distribution. Using the statistical model described above, DEGseq proposes a new method based on MA-plot [29], which was widely used in the processing of microarray data, by letting C1 and C2 denote the number of reads from a specific gene obtained from two samples, and they conform to the Ci ~ binomial(ni,pi), i = 1,2 distribution, where ni denotes the number of reads on all the comparison total number of reads, and pi denotes the probability of being from that gene.DEGseq defines M = log2C1-log2C2 and A = (log2C1 + log2C2)/2 and demonstrates that under the assumption of random sampling, the conditional distribution M, given A = a (a is the observed value of A), follows an approximately normal distribution. For each gene on the MA plot, a hypothesis test H0: p1 = p2 versus H1: p1 ≠ p2 was performed. p-values were then calculated based on the normal distribution, and the p-values were corrected to Q-values.To improve the accuracy of differential circRNAs [30], we defined that we would differentiate multiplicity of difference by more than a factor of two and with a Q-value ≤ 0.001 circRNAs, screened as significantly differentially expressed circRNAs.

Gene Ontology GO functional analysis of differential circRNA-derived genes

Based on the GO annotation results and the official classification, we functionally categorized the genes of differential circRNA sources [31], and also used the phyper function in the R software to perform enrichment analysis. p-value was calculated as shown in Fig. 4, and then the p-value was corrected by the q-value, and the functional classes with a q-value of ≤ 0.01 were usually regarded as significantly enriched [32].

KEGG functional analysis of differential circRNA-derived genes

According to the KEGG annotation results and the official classification, we classified the differential circRNA-derived genes into biological pathways, and also used the phyper function in the R software to perform enrichment analysis. p-value was calculated as shown in Fig. 5, and then q-value correction was applied to the p-value, and the pathways with a q-value ≤ 0.01 were usually regarded as significantly enriched [33].

qRT-PCR validation

After RNA-seq analysis, qRT-PCR validation was performed on the significantly differentially expressed genes that had been screened. we selected five differentially expressed circRNAs (novel_circ_034906, novel_circ_043550, novel_circ_061688, novel_circ_056122, novel_circ_035243) were validated by qRT-PCR. The primer sequences of each differentially expressed gene are detailed in Table 1.

Construction of circRNA-miRNA-mRNA relationship network

RNAhybrid database and miRanda database were used to predict the miRNAs that circRNAs may bind [34, 35], and then the downstream mRNA target genes of miRNAs are predicted in Targetscan database, and the final regulatory genes of miRNAs are determined by intersection analysis [36]. The circRNA-miRNA-mRNA relationship network was constructed based on the ceRNA theory [37, 38], and the circRNA relationship network was visualized and displayed using Cytoscape software.

$$P = 1 - \sum_{i=0}^{m-1} \frac{\binom{M}{i}\binom{N-M}{n-i}}{\binom{N}{n}}$$

Fig. 5 Method of p-value calculation

Statistical analysis

Data were expressed as mean ± standard deviation (mean ± SD), and statistical processing was performed using SPSS 29.0 software. One-way analysis of variance (ANOVA) was used: if the variance was homogeneous, the test was performed using the LSD method; if the variance was not homogeneous, the test was performed using the Games-Howell method. Statistical significance was indicated when $P < 0.05$.

Results

Establishment of MIRI model in mice

The construction process of mouse MIRI model is shown in Fig. 1. The construction effect of MIRI model was confirmed by observing the changes of electrocardiogram, myocardial markers detection, cardiac color Doppler ultrasound function detection, myocardial histopathological examination, mitochondrial function and other indicators.

Mouse cardiac ultrasound results

Using the small animal ultrasound system to monitor the cardiac function indexes of the four groups of mice after modeling, compared with the Sham group, the SV, CO, LVEF and LVFS of the MIRI group, the MIRI + AICAR group, and the MIRI + Compound C group decreased ($P < 0.05$), compared with the MIRI group, the SV, CO, LVEF and LVFS increased ($P < 0.05$) and SV, CO, LVEF and LVFS decreased ($P < 0.05$) in the MIRI + Compound C group, as shown in Fig. 6. Echocardiographic observation in the four groups of mice showed that the heart chambers became larger and the contraction of the anterior wall of the left ventricle became smaller in the MIRI group compared with the Sham group, the heart chambers became smaller and the contraction of the anterior wall of the left ventricle became larger in the MIRI + AICAR group compared with the MIRI group, and the heart chambers became larger and the contraction of the anterior wall of the left ventricle was smaller in the MIRI + Compound C group compared with the MIRI group, as shown in Fig. 7.

Table 1 qRT-PCR primer sequences of AMPK-related differential circRNAs

Name	Forward primer(5′-3′)	Reverse primer(5′-3′)	Product(bp)
novel_circ_034906	ATAAGTCTGTGCTTGCAGCTCGA	CCAGGCAGAGGTGGAGTAGGTT	164
novel_circ_043550	TACCATCGGCCCAAACCCT	GTTGAGGTCAGTGAACATCCGAA	107
novel_circ_061688	TGTATATGCAGCTAGATGAGGGAAG	GTTCTCTGCTGAGGTAGCCTGTCT	146
novel_circ_056122	GCTGAATACCAGTCATTGTGTCCTC	GCTGTATCAAAGTAGCACTCGCG	218
novel_circ_035243	TCGGCGAACTGAACAGCATG	TAGAAGAGGCTGATGACTGGGAG	105

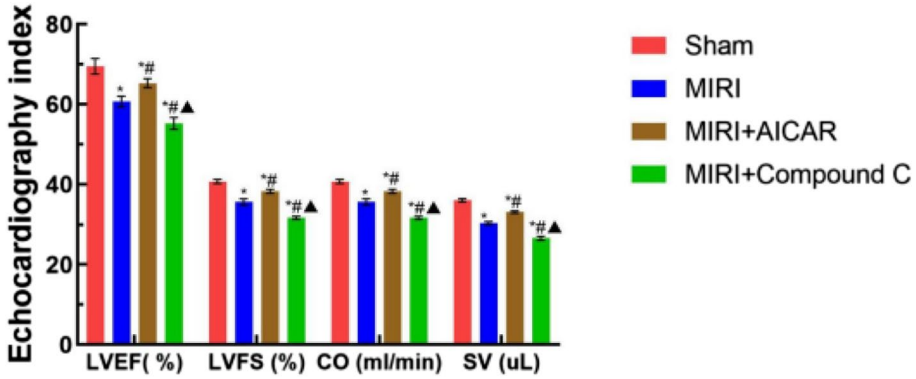

Fig. 6 Comparison of cardiac function parameters among the four groups of mice, the X-axis represents the cardiac ultrasound indexes, and the Y-axis represents the values of the indexes, which are expressed as the mean ± standard deviation, compared with the Sham group, *$p < 0.05$, with statistical difference; compared with the MIRI group, # $p < 0.05$, with statistical difference; compared with the MIRI + AICAR group, ▲$p < 0.05$, with statistical difference

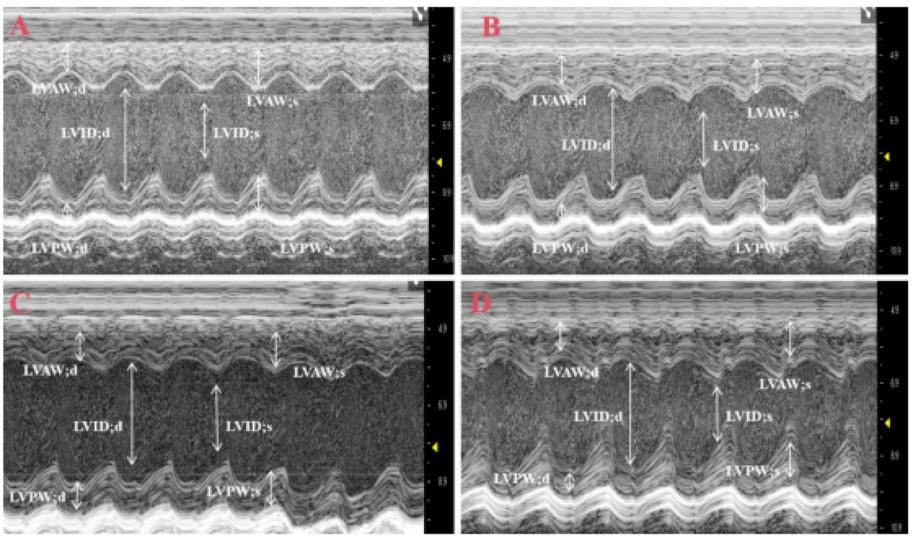

Fig. 7 M-mode ultrasound patterns of the morphology structure and systolic function of the left ventricle in mice (A: Sham group, the shape of the cardiac chambers was regular, and the beat was strong; B: MIRI group, the cardiac chambers become larger and the contraction amplitude of the anterior wall of the left ventricle becomes smaller than that of the Sham group; C: MIRI + AICAR group, the cardiac chambers become smaller and the contraction amplitude of the anterior wall of the left ventricle becomes larger than that of the MIRI group; D: MIRI + Compound group, compared with the MIRI group, the cardiac chambers became larger and the contraction amplitude of the anterior wall of the left ventricle became smaller.White arrows are left ventricular internal end-diastolic diameter (LVID; d), left ventricular internal end-systolic diameter (LVID; s), Left ventricular end-diastolic posterior wall thickness (LVPW; d), Left ventricular end systolic—posterior wall thickness, LVPW; s); Left ventricular end-diastolic anterior wall thickness (LVAW; d); Left ventricular end-systolic anterior wall thickness (LVAW; s))

Results of serum myocardial markers

Serum myocardial marker levels were measured using the enzyme linked immunosorbent assay (ELISA) method, and BNP, CK-MB, and CTnT increased in the MIRI group, the MIRI + AICAR group, and the MIRI + Compound C group compared with the Sham group ($P < 0.05$), and BNP, CK-MB, and CTnI decreased in the MIRI + AICAR group compared with the MIRI group ($P < 0.05$). BNP, CK-MB, and CTnI decreased in the MIRI + AICAR group ($P < 0.05$) and increased in the MIRI + Compound C group ($P < 0.05$) compared to the MIRI + AICAR group ($P < 0.05$) (as shown in Fig. 8).

HE staining results

The results of HE staining showed that the cardiomyocytes in Sham group were arranged in a regular manner, the nuclei of the cells were obvious, and there was no inflammatory cell infiltration; the myocardial tissue in

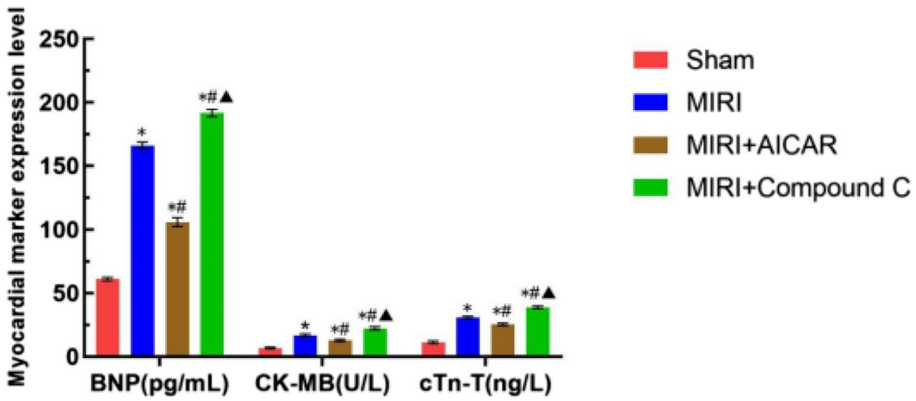

Fig. 8 Comparison of serum myocardial marker results in four groups of mice, X-axis represents serum myocardial marker indexes, Y-axis represents the values of the indexes, expressed as mean ± standard deviation, compared with the Sham group, *$p < 0.05$, statistically different, compared with the MIRI group, # $p < 0.05$, statistically different, compared with the MIRI + AICAR group, ▲$p < 0.05$, statistically different

MIRI group showed limited necrosis of cardiomyocytes, disordered arrangement of myocardial fibers and a small amount of inflammatory cell infiltration; the cardiomyocytes in the MIRI + AICAR group were arranged in an orderly manner, and the degree and scope of necrosis of the cells were lower than those in the MIRI group; the cardiomyocytes in the MIRI + Compound C group had a more disorganized arrangement of cardiomyocytes, a greater extent of cell necrosis, and a large number of inflammatory cell infiltration than the MIRI group. As shown in Fig. 9.

Ultra-microscopic cardiomyocyte morphology results

Under transmission electron microscopy, the myofibers of cardiomyocytes in the Sham group were neatly arranged, with abundant mitochondria in the cytoplasm, which were located next to the nucleus and between the bundles of myofibrils, and were round or oval in shape. Compared with the Sham group, cardiomyocyte myofibers in the MIRI group were sparse, mitochondria were swollen and degenerated, disordered and piled up, and cristae disintegrated, and the MIRI + AICAR group showed significant improvement compared with the

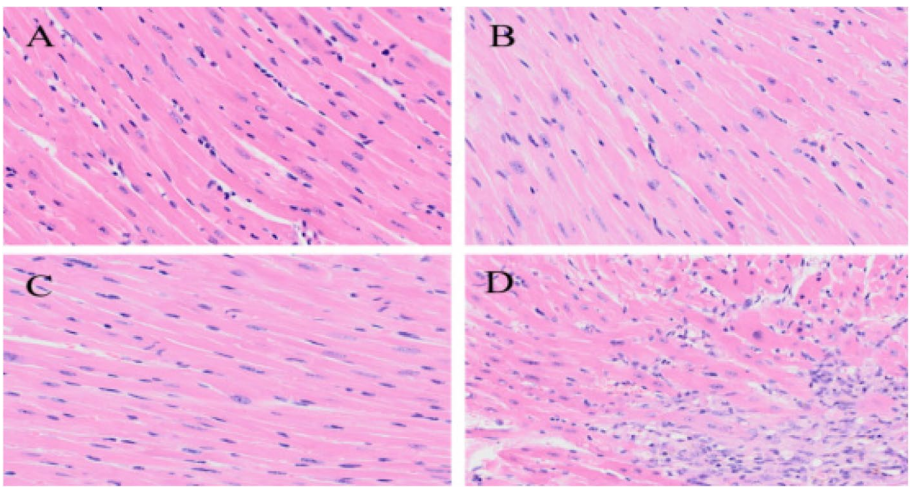

Fig. 9 Comparison of HE staining results of cardiomyocytes in four groups of mice (A: Sham group, cardiomyocytes were regularly arranged, with obvious nuclei; B: MIRI group, limited cardiomyocyte necrosis, and disorganized arrangement of myocardial fibers; C: MIRI + AICAR group, cardiomyocytes were arranged in an orderly manner, and the degree and extent of cellular necrosis were lower in comparison to MIRI group D: MIRI + Compound C group, more disorganized, and a large amount of inflammatory cell infiltration in comparison to MIRI group). MIRI group, the arrangement of cardiomyocytes was more disorganized, the extent of cell necrosis was larger, and a large number of inflammatory cells were infiltrated)

MIRI group, with basically normal myocardial fiber structure and well-arranged myofibrillar fibers, mitochondrial swelling, and myocardial injury was reduced compared with that of the MIRI group, and the MIRI + Compound C group was more sparse and well-arranged compared with that of the MIRI group. MIRI + Compound C group was significantly reduced compared with the MIRI group. Myocardial fibers of cardiomyocytes were sparse, and mitochondria in the cytoplasm were swollen and disorderly. As shown in Fig. 10.

Screening of differential circRNA source genes

A total of 68,855 genes were predicted by RNA-seq sequencing, and 315 genes were significantly differentially expressed, of which 90 were up-regulated,225 were down-regulated. The statistical results of the differential circRNAs are shown in Fig. 11. Volcano-plot and Scatter-plot were also used to show the distribution of differential circRNAs in the MIRI group versus the MIRI + AICAR group, and the MIRI group versus the MIRI + Compound C group, and expression heatmaps were made for each group of the differential comparison scheme, which are shown in Fig. 12, Fig. 13 and Fig. 14, respectively.

GO function analysis of differential circRNA-derived genes

The differentially expressed circRNAs from the MIRI group and the MIRI + AICAR group, and the MIRI group and the MIRI + Compound C group were subjected to GO functional analysis, which was a database established by the Gene Ontology Consortium, describe the roles of genes and proteins in cells by creating a set of controlled vocabulary with dynamic forms, thus comprehensively describing the attributes of genes and gene products in organisms. GO was divided into three major functional categories, namely, molecular function, cellular component, and biological process. In the GO function analysis, there were 27 types of GOs enriched in the MIRI group compared with the MIRI + AICAR group, and 29 types of GOs enriched in the MIRI group compared with the MIRI + Compound C group. The GO classification results of differentially expressed circRNAs were shown in Fig. 15, and the GO function classification up- and down-regulation statistics of differentially expressed circRNAs are shown in Fig. 16.

Pathway functional analysis of differential circRNA-derived genes

Using DEGs, we performed KEGG pathway classification and functional enrichment, including illustrated information on cellular biochemical processes such as metabolism, membrane translocation, signaling, and cell cycle. The genes were categorized into six branches according to the KEGG metabolic pathways involved: Cellular Processes, Environmental Information Processing, Genetic Information Processing, Human Disease (HDP),Metabolism, and Organismal Systems. In order to analyze the pathological pathway of action of the differential genes more further, enrichment analysis was performed between two comparison groups, the MIRI group and the MIRI + AICAR group and the MIRI group and the MIRI + Compound C group, to obtain the Pathway of the enriched differential genes. As shown in Fig. 17.

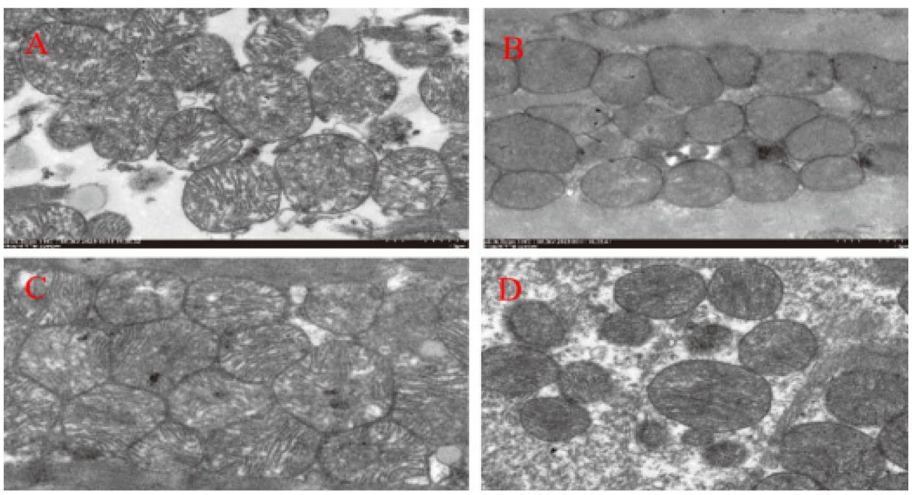

Fig. 10 Comparison of myocardial mitochondrial morphology under ultramicroelectron microscopy in four groups of mice (A: Sham group, myofibrils were neatly arranged, mitochondria were regular in morphology and abundant in number; B: MIRI group, myofibrils were sparse, mitochondria were swollen and denatured, and cristae disintegrated and disappeared; C: MIRI + AICAR group, myofibrils were basically structurally normal, and mitochondria were mildly swollen; D: MIRI + Compound C group. Myofibers are sparse, mitochondria are swollen and disordered in arrangement)

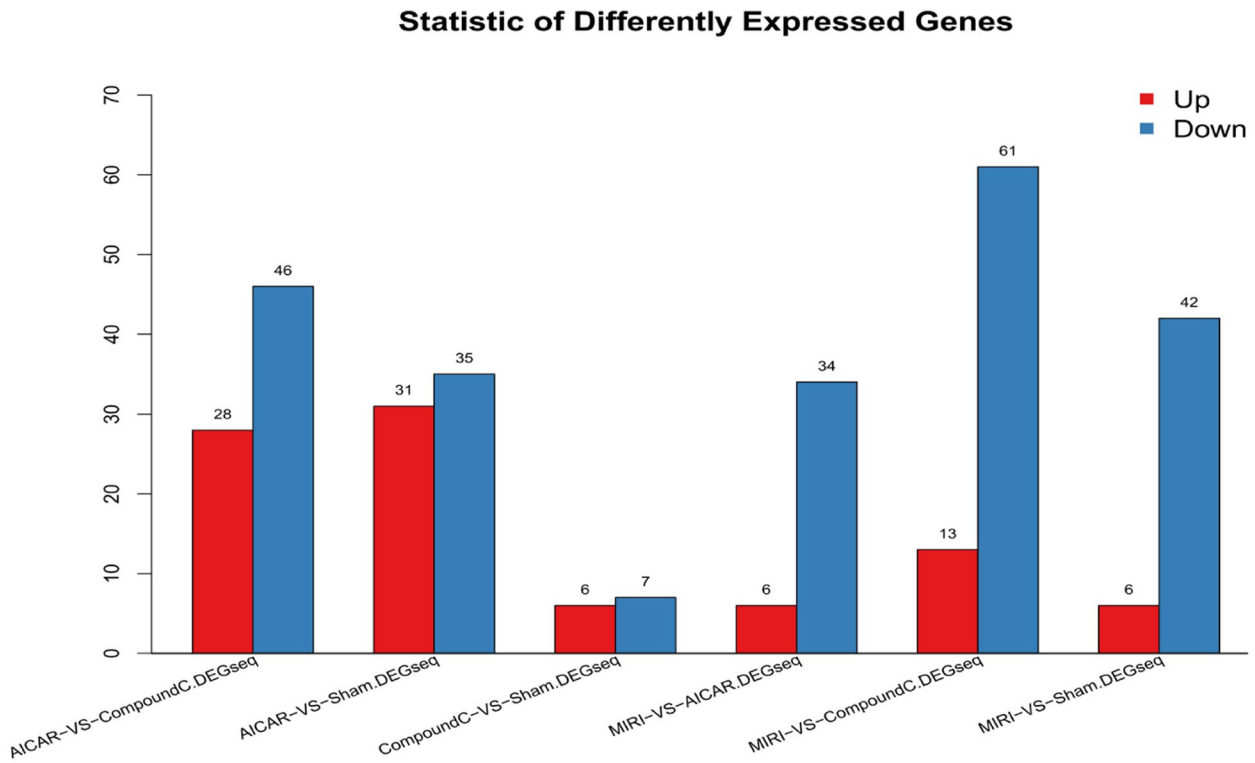

Fig. 11 Statistical plots of the number of differentially expressed circRNAs in the MIRI group versus the MIRI + AICAR group, and in the MIRI group versus the MIRI + Compound C group (X-axis represents the differential comparison scheme for each group, and the Y-axis represents the number of the corresponding differential circRNAs. Red color represents the number of up-regulated circRNAs and blue color represents the number of down-regulated circRNAs)

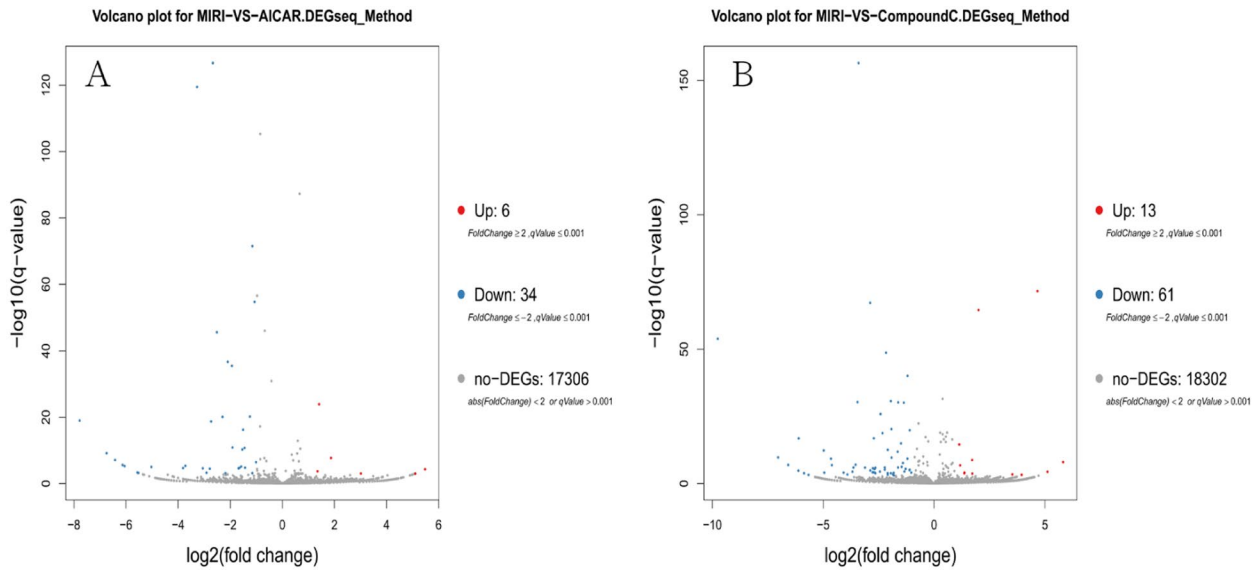

Fig. 12 Volcano-plot distributions of differentially expressed circRNAs in the MIRI group versus the MIRI + AICAR group, and the MIRI group versus the MIRI + Compound C group (X-axis represents log2-transformed differential multiplicity values, and Y-axis represents -log10-transformed significance values. Red represents up-regulated circRNAs, blue represents down-regulated circRNAs, and gray represents non-differentially expressed circRNAs)

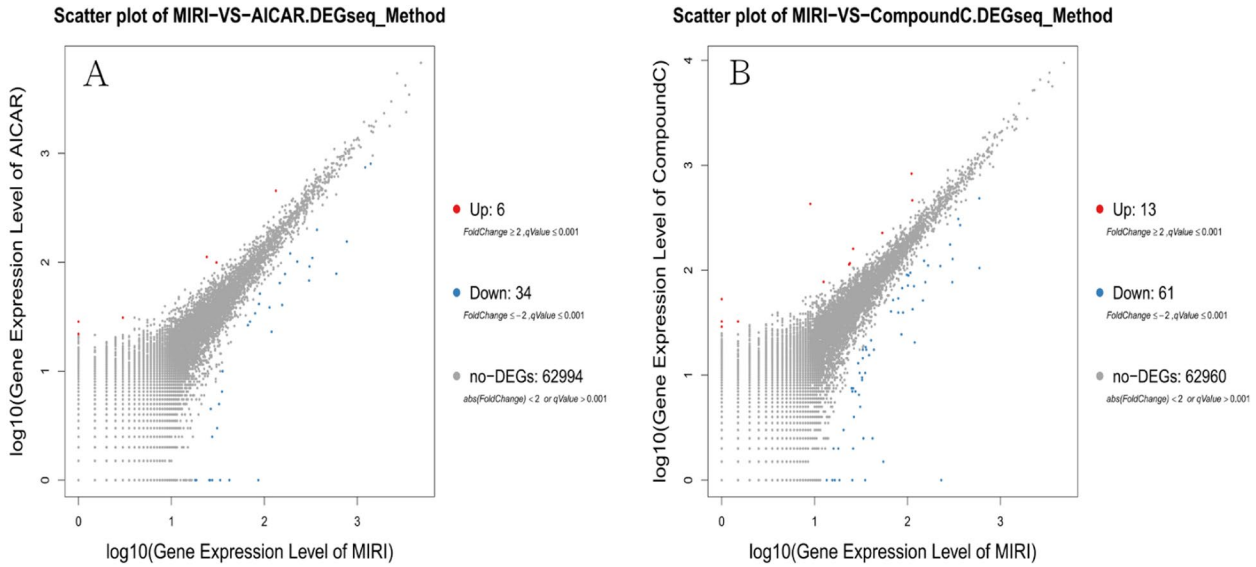

Fig. 13 Scatter-plot distributions of differentially expressed circRNAs in the MIRI group versus the MIRI + AICAR group, and in the MIRI group versus the MIRI + Compound C group (X and Y axes both represent logarithmic values of circRNA expression. Red represents up-regulated circRNAs, blue represents down-regulated circRNAs, and gray represents non-differentially expressed circRNAs)

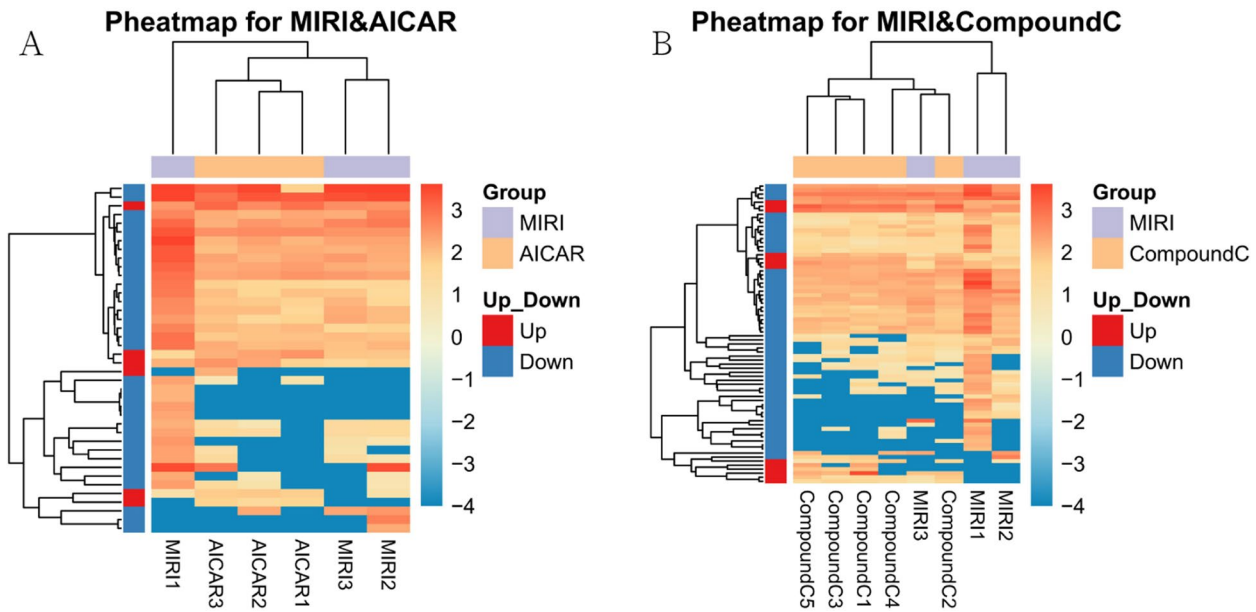

Fig. 14 Heatmap of the expression of differentially expressed circRNAs in the MIRI group versus the MIRI + AICAR group, and the MIRI group versus the MIRI + Compound C group (X-axis represents the samples for clustering analysis, and Y-axis represents the differentially circRNAs. the colors represent the log10-transformed expression, with darker colors indicating higher expression and lighter colors indicating lower expression)

Validation of differentially expressed genes

Through bioinformatics analysis and screening, the genes novel_circ_034906, novel_circ_043550, novel_circ_061688, novel_circ_056122, novel_circ_035243 were found to be the key genes in the development of MIRI In order to verify these genes, we used qRT-PCR to detect the relative expression levels of the target genes. The five genes were all down-regulated in MIRI + AICAR group and up-regulated in MIRI + Compound C group ($P < 0.05$), which was

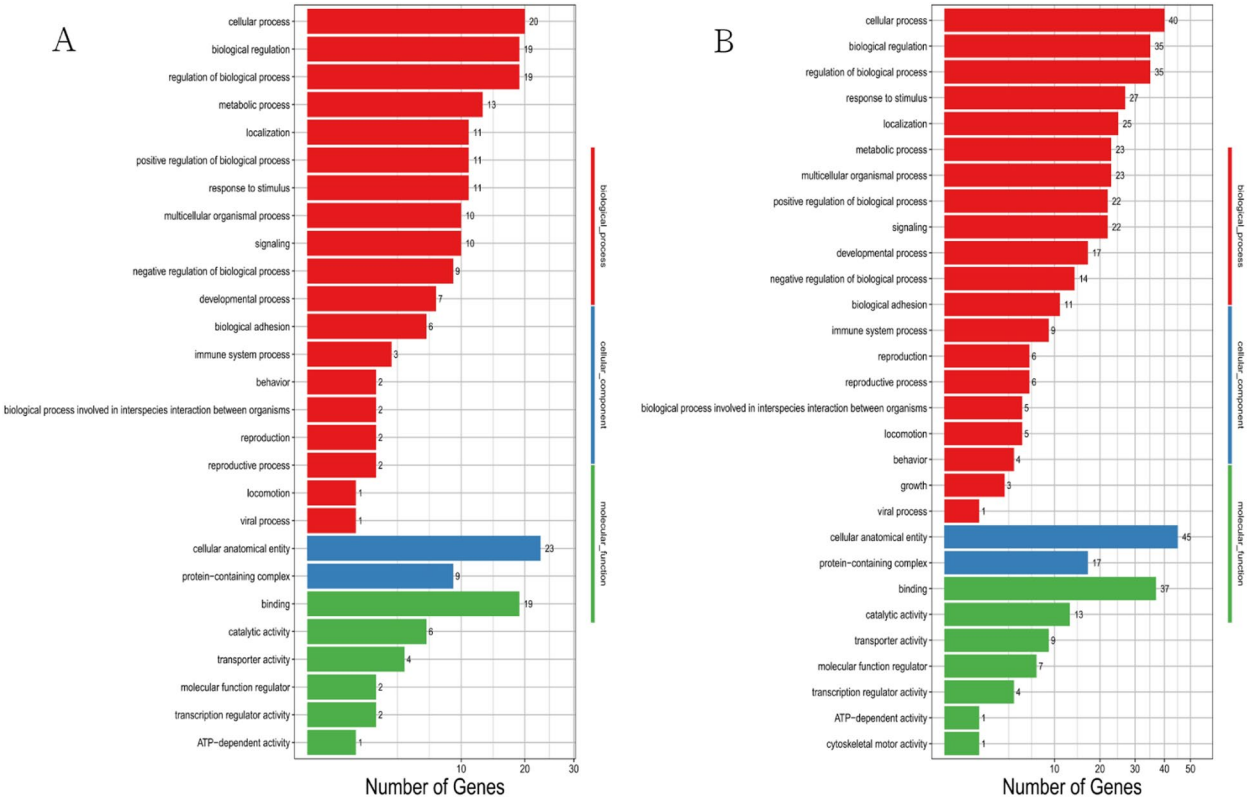

Fig. 15 GO functional classification plots of differentially expressed circRNAs. panel A shows the GO functional classification of DEGs between the MIRI group and the MIRI + AICAR group, and panel B shows the GO functional classification of DEGs between the MIRI group and the MIRI + Compound C group, Calcium Channel Activity (GO:0005262, $p = 0.01950$), Cation Channel complex (GO:0034703, $p = 0.01402$), transporter protein complex (GO:1,990,351, $p = 0.02181$), and postsynaptic specialization (GO:0099572, $p = 0.03244$), and the related GO functional enrichment was significant, suggesting that these types of GO functional classifications are involved in the mechanism of MIRI, (X-axis represents the differentially expressed number of circRNA-derived genes, Y-axis represents GO functional classifications)

consistent with the change trend of RNA-seq results. The accuracy of RNA-seq results was confirmed, which supported the reliability and scientific nature of the results of this study, as shown in Fig. 18. Differentially expressed genes were therefore included in subsequent analyses.

Construction of circRNA-miRNA-mRNA relationship network

In order to further speculate the possible biological functions of differential circrnas, two differential target genes (novel_circ_043550 and novel_circ_035243) verified by qRT-PCR were selected to predict the source genes of circrnas and the target genes of mirnas. Then, the downstream target gene mRNA of miRNA was predicted in the Targetscan database, and the circRNA-miRNA-mRNA relationship network consisting of 2 circrnas, 28 mirnas and 229 mrnas was finally constructed, as shown in Fig. 19.

Discussion

Ischemic Heart Disease (IHD) is the leading cause of cardiovascular disease death. At present, the number of patients with ischemic heart disease in the world has reached 125 million, and its incidence is still increasing. It seriously endangers human life safety [3, 39]. At the same time, the number of people receiving reperfusion therapy to open occluded coronary arteries due to myocardial ischemia is also increasing, and MIRI is an important pathophysiological mechanism causing heart dysfunction after coronary thrombolysis, coronary intervention surgery and CPB open heart surgery [1, 2]. Therefore, reducing or eliminating this damage has been one of the urgent problems to be solved in the cardiovascular field.

Activated AMPK can sense the changes of energy metabolism status of cells, participate in a variety of metabolic processes in cells, and is a sensor to maintain the energy balance in cells [13]. The relationship between AMPK and the development of MIRI can also be found in recent studies. For example, WANG[40]

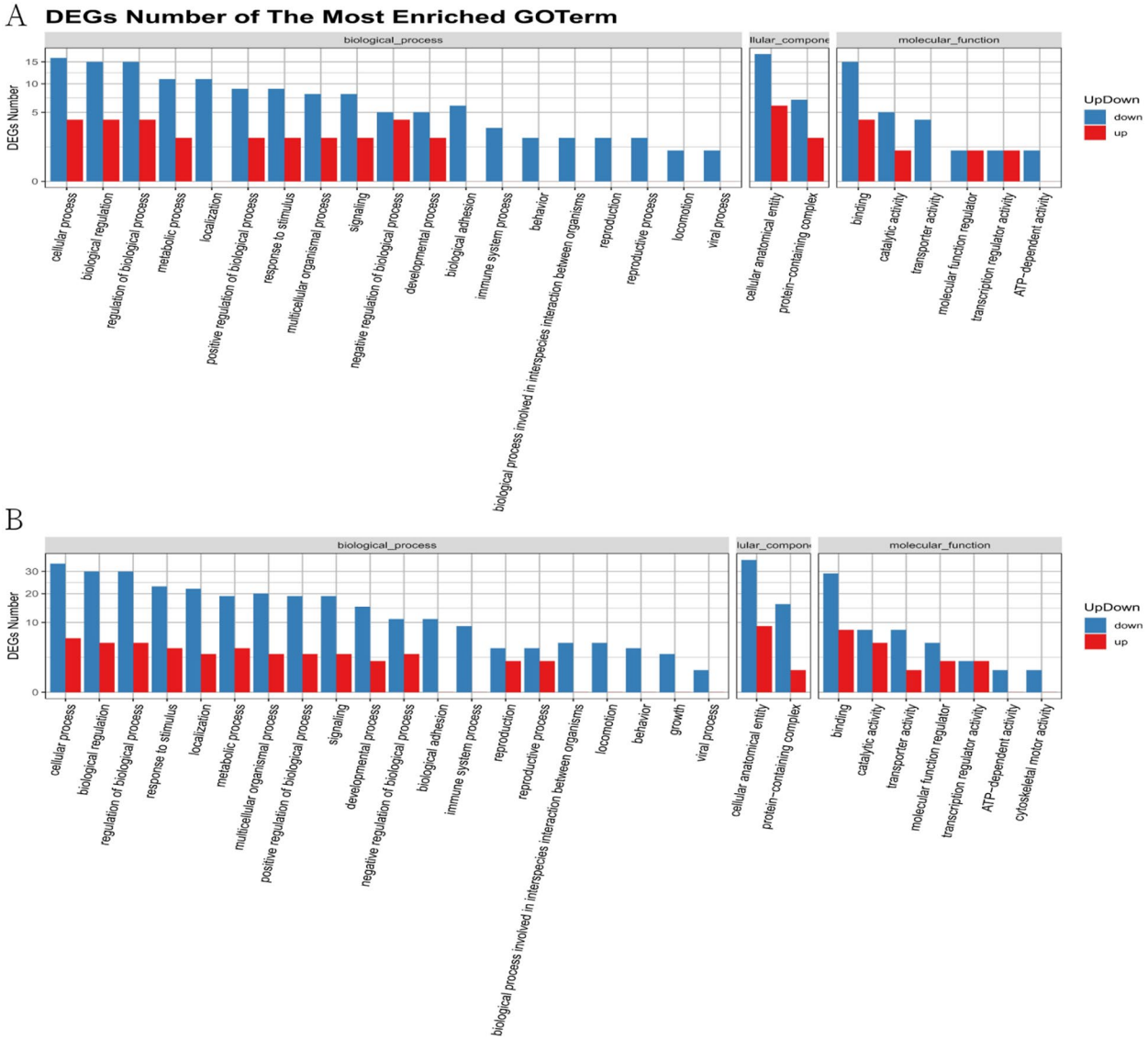

Fig. 16 Statistical plots of GO functional classification of differentially expressed circRNAs. A graph shows the statistics of up- and down-regulation of GO functional classification of differentially expressed circRNAs between the MIRI group and the MIRI + AICAR group, and B graph shows the statistics of up- and down-regulation of GO functional classification of differentially expressed circRNAs between the MIRI group and the MIRI + Compound C group (X-axis represents the GO functional classification, and Y-axis represents the number of up- and down-regulated circRNA source genes in the corresponding GO classification)

et al. found that dexmedetomidine can reduce MIRI induced iron apoptosis through AMPK/GSK-3β/Nrf 2 axis. TIAN et al. [4] showed that Tilianin pretreatment could improve mitochondrial energy metabolism and oxidative stress through AMPK/SIRT 1/ PGC-1α signaling pathway in MIRI rats. LI et al. [41] suggested that genipin could reduce MIRI by inhibiting NLRP 3 inflammasome-mediated apoptosis through AMPK signaling pathway. DU et al. [42] showed that activation of AMPK could reduce MIRI by regulating DRP1-mediated mitochondrial dynamics. YIN et al. [43] suggested that AMPK is a key regulatory molecule in age-related MIRI. Comprehensive previous studies have found that AMPK, as an important molecule in the regulation of mitochondrial function, has endogenous myocardial protective effect and can be regulated in three ways: First, the peroxlsome proliferator-activated receptor-γ coactlvator-1α (PGC-1α) is phosphorylated after AMPK activation. In turn, nuclear respiratory factor-1/2 (NRF-1/2) is activated, Mitochondrial DNA (mtDNA) replication is increased, and mitochondrial biosynthesis is promoted, thus playing a protective effect on myocardium [9].

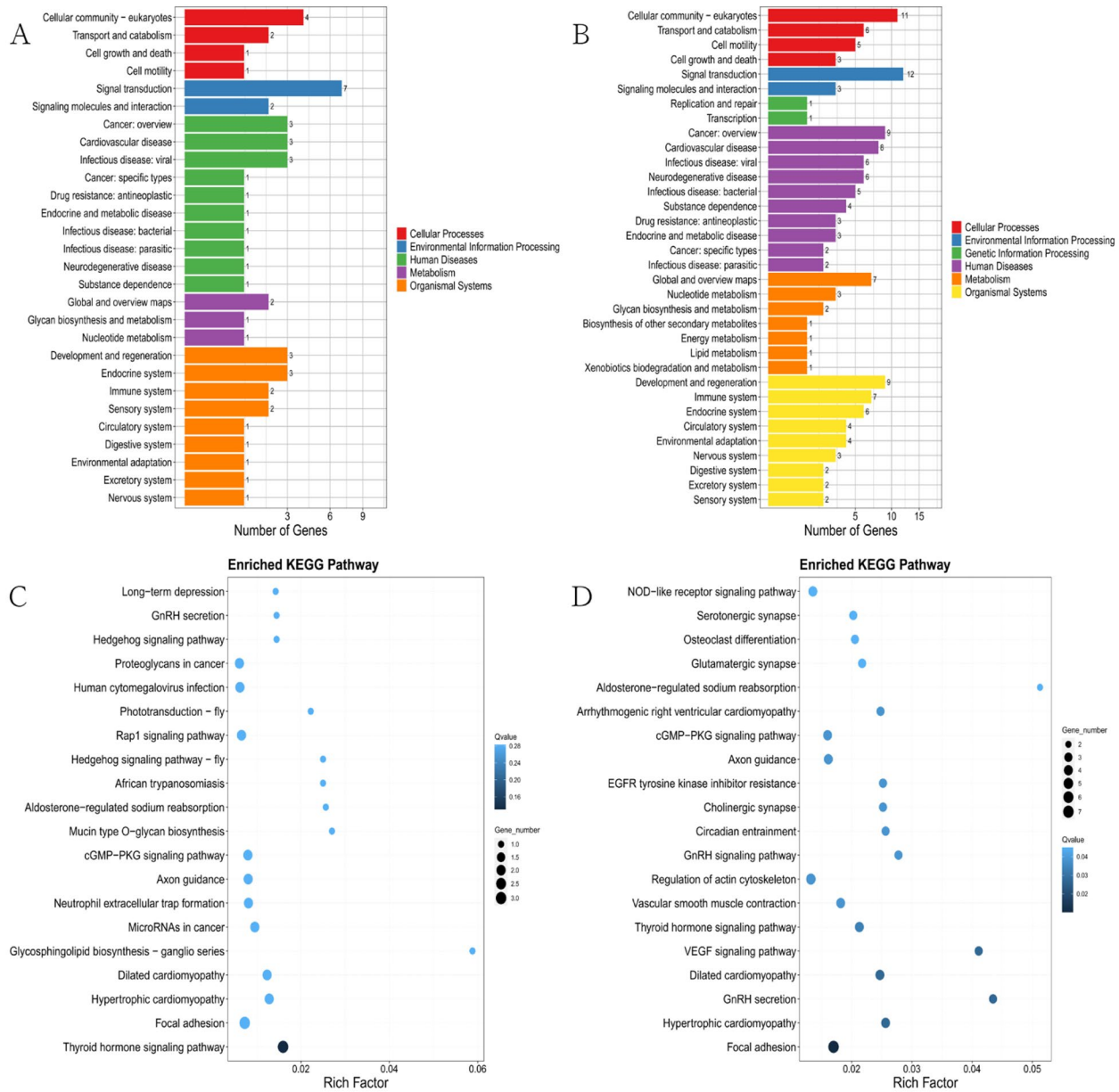

Fig.17 A graph shows the Pathway classification of differentially expressed circRNAs between the MIRI group and the MIRI + AICAR group, B graph shows the Pathway classification of differentially expressed circRNAs between the MIRI group and the MIRI + Compound C group (the X-axis represents the proportion of genes accounted for, and the Y-axis represents the classification of KEGG function), C graph shows the Pathway enrichment results of differentially expressed circRNAs between the MIRI group and MIRI + AICAR group, D graph shows the Pathway enrichment results of differentially expressed circRNAs between MIRI group and MIRI + Compound C group (X-axis represents the enrichment factor value, Y-axis represents the pathway name. Red boxes were filtered functional categories and pathway names. The color represents the q-value (the whiter the color the larger the value, the bluer the smaller the value), the smaller the value represents the more significant enrichment result. The size of the dots represents the number of differential circRNA source genes (the larger the dot represents the larger the number, the smaller represents the smaller the number).RichFactor refers to the enrichment factor value, which was the quotient of the foreground value of a pathway on the annotation (the number of differential circRNA source genes) and the background value of a pathway on the annotation (the number of all circRNA source genes), and the larger the value, the more obvious the enrichment result was. indicates the more obvious enrichment results

Second, mitochondrial fission is mainly mediated by dynamic related protein1 (Drp1) and mitochondrial fissionfactor (Mff). Excessive Mitochondrial fission can cause the opening of Mitochondrial permeability transition pore (mPTP) and the release of ROS, which leads to the activation of mitochondrial pathway myocardial

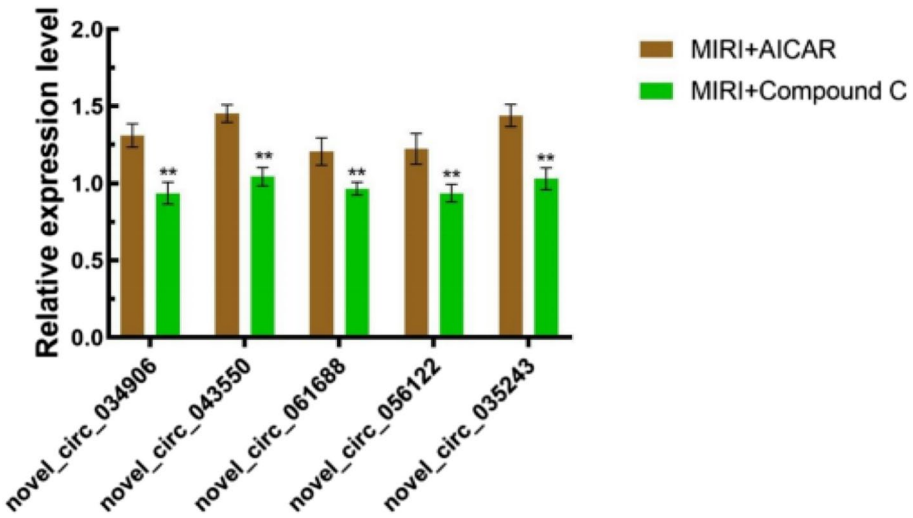

Fig. 18 Relative qRT-PCR expression results of differentially expressed circRNAs, X-axis represents differentially expressed genes, Y-axis represents gene expression, expressed as mean ± standard deviation, and ** indicates $p < 0.01$, statistically different

apoptosis, which is an important factor affecting myocardial injury [10, 44]. Thirdly, mitophagy is a special autophagy mode and defense mechanism, which is a process of mitochondrial self-renewal and selective removal of damaged mitochondria in cells [12, 45]. Therefore, timely removal of damaged mitochondria is extremely important for reducing abnormal accumulation of ROS, maintaining mitochondrial ATP generation function and the stability of cellular metabolic microenvironment [11]. The activation of autophagy initiation molecule UNC-51-like kinase 1 (ULK1) is a key molecule regulating autophagy. Activation of AMPK can promote the activation of ULK1, thereby inducing mitophagy, efficiently removing damaged mitochondria and reducing the generation of ROS. Maintenance of ATP synthesis and metabolic homeostasis in cardiomyocytes [12, 46]. Moreover, AICAR, an activator of AMPK, can effectively increase myocardial ATP content and alleviate myocardial injury by promoting AMPK activation. Exogenous recombinant adiponectin also has the effect of activating AMPK, and can improve myocardial metabolic disorders and promote the recovery of cardiac function after ischemia–reperfusion [13]. The previous research results of our research group also proved the above conclusion. AMPK maintains the dynamic balance of myocardial mitochondrial function through the regulation of mitochondrial function through cohesion, and plays an anti-MIRI effect by inhibiting the abnormal accumulation of ROS and promoting the production of mitochondrial ATP [13, 46].

However, the current prevention and treatment drugs and strategies for MIRI still have not achieved very ideal results in clinical practice. There may be other unrecognized or valued factors involved, such as circRNA and other previously neglected ncRNA, which need to be further explored in MIRI [14]. circRNA, a new member of the non-coding RNA family [47, 48], is a class of ncRNA with covalently closed loops formed through reverse cleavage of pre-mRNA [49]. circRNA plays a regulatory role at transcriptional and post-transcriptional levels, and is involved in various cardiovascular physiological and pathological processes such as embryo formation, cardiovascular development, heart failure, myocardial hypertrophy, myocardial fibrosis and myocardial apoptosis [50]. Recent studies [51–55] have shown that some circrnas in myocardial cells are involved in the regulation of mitochondrial function. For example, circRNATtc3 is significantly increased in the myocardium of ischemia and hypoxia, and circRNATtc3 can inhibit the dysfunction of mitochondrial ATP production induced by ischemia and hypoxia. It can effectively reduce the apoptosis of myocardial cells and myocardial ischemia–reperfusion injury [56]. For example, circRNAMFACR was significantly up-regulated in the myocardium of mice with ischemia/reperfusion, which adsorbed miR-652-3p through the "sponge" mechanism, and then increased myocardial mitochondrial fission and cardiomyocyte apoptosis. Further, after knocking down the expression of circRNAMFACR in the myocardium by adenovirus transfection, the expression of circrnamFACR in the myocardium was down-regulated. It reduces the adsorption of circRNA to miR-652-3p, thereby inhibiting the expression of mitochondrial membrane protein MTP18, thereby reducing the division of myocardial mitochondria and the size of myocardial infarction in mice with ischemia–reperfusion [57]. The above studies suggest that circrna may play an important role in the mechanism of MIRI. Some specific

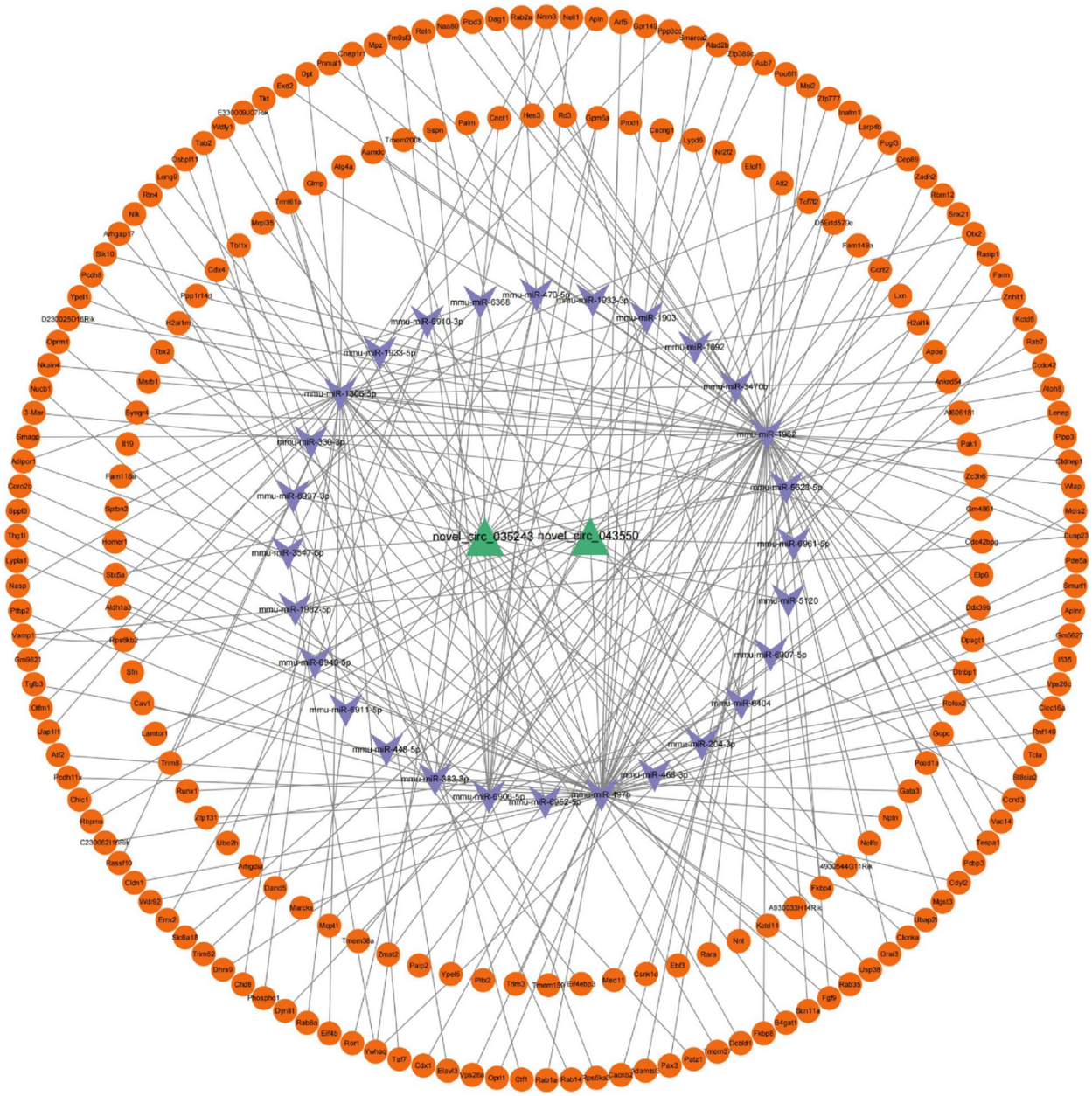

Fig. 19 circRNA-miRNA-mRNA relationship network, green represents circRNAs, purple represents miRNAs, and orange represents mRNAs

circRNA molecules in response to AMPK activation may be involved in this process and play an important role. Since AMPK is a central molecule in the regulation of mitochondrial function, the regulatory effects of these circrnas may be closely related to AMPK. By reviewing the literature, we found that some circrnas that respond to AMPK activation play a role in the occurrence and development of non-cardiac diseases. For example, CircRNA_002581 is involved in the pathogenesis of alcoholic liver disease through PTEN-AMPK-mTOR pathway related autophagy inhibition [58]. Ampk-mediated circPRKAA 1 plays a role in the occurrence and development of hepatocellular carcinoma [59–61]. Some researchers have also found that circLARP 1B promotes the synthesis of fatty acids in hepatocellular carcinoma and promotes cell metastatic characteristics and lipid accumulation through the HNRNPD-LKB 1-AMPK pathway. Circulus WIM 6 plays a key role in mammalian hepatocellular carcinoma [62]. In addition, Gong et al. [62] revealed that Circulus WIm 6 plays an important

role in age-related osteoarthritis by regulating extracellular matrix metabolism and AMPK related energy metabolism. Circulus WIM 6-RPS 14-PCK 1-AMPK axis is a potential biomarker for osteoarthritis. Therefore, we wonder whether some specific circRNA in response to AMPK activation is involved in the regulatory network of myocardial mitochondrial function in ischemia–reperfusion and is involved in the regulation of MIRI. At present, there are few reports in the world, so it is of potential research significance to focus on the above scientific issues for in-depth research. Therefore, in this study, the mouse MIRI model was constructed, and the differentially expressed circRNA related to AMPK in MIRI was screened by bioinformatics technology, and the AMPK-related circRNA regulatory network was constructed to explore the possible regulatory role of circRNA in AMPK-mediated myocardial mitochondrial function after ischemia–reperfusion. This study provides a possible research basis for finding the potential circRNA diagnostic markers of MIRI.

In this study, the changes of cardiac morphology and cardiac function parameters, serum myocardial marker levels, pathological staining results, and the number of mitochondrial morphology results under electron microscopy were analyzed. Interestingly, the application of AMPK agonist and AMPK inhibitor in the corresponding groups produced different experimental effects. After high-throughput sequencing of mouse myocardial tissue, the differentially expressed circRNA was detected by DEGseq algorithm, and a total of 68,855 genes were predicted. Among them, 315 genes were significantly differentially expressed, of which 90 were up-regulated and 225 were down-regulated. Five differentially expressed circrnas were screened, among which novel_circ_034906 predicted transcription factor activity for DNA binding, RNA polymerase II specificity, and RNA polymerase II transcriptional regulatory region sequence-specific DNA binding activity [63]. It is involved in the regulation of nervous system development and the proliferation of neural precursor cells [64]. novel_circ_043550 encodes a ubiquitin-binding protein required for the regulation of mitochondrial size and clearance. It is an essential gene required for autophagy, mitochondrial size and clearance in Drosophila. novel_circ_061688, as a DNA fragment, may be related to eukaryotic neural tube defects [65]. novel_circ_056122 is a member of the protocadherin β gene cluster, which can promote ferroapoptosis and is a new tumor suppressor in hepatocellular carcinoma [66]. novel_circ_035243 is an important gene involved in fat regulation and energy metabolism in Drosophila [67]. The results of qRT-PCR showed that 5 differential target genes were down-regulated in MIRI + AICAR group and up-regulated in MIRI + Compound C group, which was consistent with the results of RNA-seq. Considering the correlation between MIRI and mitochondrial energy metabolism in this study, two differential circrnas (novel_circ_043550 and novel_circ_035243) were selected from the above five differential genes for the construction of AMPK-related circRNA relationship network. Firstly, target gene prediction analysis of miRNA was performed on the source gene of differential circRNA, and then the downstream target gene mRNA of miRNA was predicted in Targetscan database. Finally, a circRNA-miRNA-mRNA network consisting of 2 circRNA, 28 miRNA and 229 mRNA was constructed. Bioinformatics analysis showed that these two circrnas (novel_circ_043550, novel_circ_035243) were associated with calcium channel activity (GO:0005262, novel_circ_035243). $p = 0.019500$), cation channel complex (GO:0034703, $p = 0.01402$), transporter complex (GO:1,990,351, $p = 0.02181$), postsynaptic specialization (GO:0099572, $p = 0.03244$) and other related functions were significantly enriched. It is speculated that differential circRNA may regulate the occurrence and development of MIRI by affecting biological processes such as cell signal transduction, mitophagy, and energy metabolism.

In conclusion, we used AMPK agonist and inhibitor intervention in mouse MIRI model, screened AMPK-related differentially expressed circRNA by bioinformatics and high-throughput sequencing, and constructed AMPK-related circRNA regulatory network in this study. However, the researchers also realized many shortcomings and defects, the first is the limitation of functional verification. Although this study constructed AMPK-related differentially expressed circrnas and constructed the regulatory network, the function of these circrnas was not directly verified, such as overexpression or knockdown experiments in vivo or in vitro. In the future, we plan to conduct functional intervention experiments of circRNA in in vitro cell model and mouse model to further verify its specific role in MIRI. The second is the selection of sample size. This study follows the ethical issues in animal research: the principles of three R's (replacement, reduction, and refinement). Based on the reports in the existing literature and combined with the limitations of actual experimental resources, we chose a sample size of 8 C57 mice per group. The expression and function of these circrnas were validated in different species to enhance the generalization and reliability of the results. Thirdly, the depth of mechanism research. This study mainly puts forward the hypothesis that circRNA may affect AMPK pathway based on ceRNA regulatory mechanism, and fails to explore other potential mechanisms in depth. In order to understand the multi-dimensional regulatory mechanism of circRNA in MIRI more comprehensively. However, its clinical application still

needs to be verified. In the future, specific circRNA may be screened in clinical samples to evaluate its expression in patients, so as to promote the potential clinical transformation of circRNA. This study provides new clues and experimental basis for the development and transformation of myocardial protective drugs based on AMPK targets.

Acknowledgements
Not applicable.

Clinical trial number
Not applicable.

Authors' contributions
Yang Song completed the framework construction of the entire manuscript and the preparation of the manuscript, Yi Zhao adjusted the text, Xiaodi Zhang and Cheng Cheng improved the text during the manuscript writing process, and the corresponding author gave guidance on the construction of ideas and the writing guidance of the whole process for the completion of the manuscript, and gave project fund support. Therefore, the authors all co-created the manuscript, reviewed the final manuscript and agreed to publish. The authors declare that they have no competing interests.

Funding
This study was supported by the National Natural Science Foundation of China [grant number 82360086、82160060] and Guizhou Provincial Science and Technology Projects ZK [2022] [grant Numbers YB669 and YB652].

Data availability
Availability of data and materials: The RNA sequencing data of this study have been uploaded to the NCBI database under the data access number GSE278398.

Declarations

Ethics approval and consent to participate
The experiment was approved by the Experimental Animal Ethics Committee of the Affiliated Hospital of Zunyi Medical University (Ethics No. zyfy-an-2023–0221).

Consent for publication
Not applicable.

Competing interests
The authors declare no competing interests.

Received: 2 September 2024 Accepted: 28 November 2024
Published online: 30 December 2024

References

1. Liu Y, Li L, Wang Z, Zhang J, Zhou Z: Myocardial ischemia-reperfusion injury; Molecular mechanisms and prevention. Microvasc Res. 2023;149:104565.
2. Dergunova LV, Vinogradina MA, Filippenkov IB, Limborska SA, Dergunov AD. Circular RNAs Variously Participate in Coronary Atherogenesis. Curr Issues Mol Biol. 2023;45(8):6682-700.
3. Algoet M, Janssens S, Himmelreich U, Gsell W, Pusovnik M, Van den Eynde J, Oosterlinck W. Myocardial ischemia-reperfusion injury and the influence of inflammation. Trends in Cardiovasc Med. 2023;33(6):357-66.
4. Tian L, Cao W, Yue R, Yuan Y, Guo X, Qin D, Xing J, Wang X: Pretreatment with Tilianin improves mitochondrial energy metabolism and oxidative stress in rats with myocardial ischemia/reperfusion injury via AMPK/SIRT1/PGC-1 alpha signaling pathway. J Pharmacol Sci. 2019;139(4):352-60.
5. Picca A, Mankowski RT, Burman JL, Donisi L, Kim JS, Marzetti E, Leeuwenburgh C: Mitochondrial quality control mechanisms as molecular targets in cardiac ageing. Nat Rev Cardiol. 2018;15(9):543–54.
6. Townsend LK, Steinberg GR. AMPK and the Endocrine Control of Metabolism. Endocr Rev. 2023;44(5):910-33.
7. Steinberg GR, Hardie DG. New insights into activation and function of the AMPK. Nat Rev Mol Cell Biol. 2023;24(4):255-72.
8. Herzig S, Shaw RJ. AMPK: guardian of metabolism and mitochondrial homeostasis. Nat Rev Mol Cell Biol. 2018;19(2):121-35.
9. Li YQ, Jiao Y, Liu YN, Fu JY, Sun LK, Su J. PGC-1α protects from myocardial ischaemia-reperfusion injury by regulating mitonuclear communication. J Cell Mol Med. 2022;26(3):593–600.
10. Quintana-Cabrera R, Scorrano L. Determinants and outcomes of mitochondrial dynamics. Mol Cell. 2023;83(6):857–76.
11. Wang S, Long H, Hou L, Feng B, Ma Z, Wu Y, Zeng Y, Cai J, Zhang DW, Zhao G. The mitophagy pathway and its implications in human diseases. Signal Transduct Target Ther. 2023;8(1):304.
12. Li A, et al. Mitochondrial autophagy: molecular mechanisms and implications for cardiovascular disease. Cell Death Dis. 2022;13(5):444.
13. Cai J, Chen X, Liu X, Li Z, Shi A, Tang X, Xia P, Zhang J, Yu P. AMPK: The key to ischemia-reperfusion injury. J Cell Physiol. 2022;237(11):4079–96.
14. Chen KY, Liu Z, Lu JH, Yang SY, Hu XY, Liang GY. The Function of Circular RNAs in Myocardial Ischemia-Reperfusion Injury: Underlying Mechanisms and Therapeutic Advancement. Cardiovasc Drugs Ther. 2024.
15. Meng X, Li X, Zhang P, Wang J, Zhou Y, Chen M. Circular RNA: an emerging key player in RNA world. Brief Bioinform. 2017;18(4):547–57.
16. Popov LD. Mitochondrial biogenesis: An update. J Cell Mol Med. 2020;24(9):4892–9.
17. Cai W, Liu L, Shi X, Liu Y, Wang J, Fang X, Chen Z, Ai D, Zhu Y, Zhang X. Alox15/15-HpETE Aggravates Myocardial Ischemia-Reperfusion Injury by Promoting Cardiomyocyte Ferroptosis. Circulation. 2023;147(19):1444-60.
18. Chen HY, Xiao ZZ, Ling X, Xu RN, Zhu P, Zheng SY. Correction: ELAVL1 is transcriptionally activated by FOXC1 and promotes ferroptosis in myocardial ischemia/reperfusion injury by regulating autophagy. Mol Med (Cambridge, Mass) 2022;28(1):96.
19. Luo C, Xiong S, Huang Y, Deng M, Zhang J, Chen J, Yang R, Ke X. The Novel Non-coding Transcriptional Regulator Gm18840 Drives Cardiomyocyte Apoptosis in Myocardial Infarction Post Ischemia/Reperfusion. Front Cell Dev Biol. 2021;9:615950.
20. Böttcher K, Longato L, Marrone G, Mazza G, Ghemtio L, Hall A, Luong TV, Caruso S, Viollet B, Zucman-Rossi J, et al. AICAR and compound C negatively modulate HCC-induced primary human hepatic stellate cell activation in vitro. Am J Physiol Gastrointest Liver Physiol. 2021;320(4):G543-g556.
21. Hou L, Zhang J, Zhao F. Full-length circular RNA profiling by nanopore sequencing with CIRI-long. Nat Protoc. 2023;18(6):1795–813.
22. Zhang L, Li X, Gao H, Li P. The Role of Circular RNA Variants Generated from the NFIX Gene in Different Diseases. Mol Pharm. 2024;21(3):1027–37.
23. Shan Y, Li J, Duan X, Zhang X, Yu J. Elucidating the multichromosomal structure within the Brasenia schreberi mitochondrial genome through assembly and analysis. BMC Genomics. 2024;25(1):422.
24. Pham M, Tu Y, Lv X. Accelerating BWA-MEM Read Mapping on GPUs. ICS : proceedings of the ACM International Conference on Supercomputing International Conference on Supercomputing. 2023;2023:155–66.
25. Gao Y, Wang J, Zhao F. CIRI: an efficient and unbiased algorithm for de novo circular RNA identification. Genome Biol. 2015;16(1):4.
26. Wegner M, Kaulich M. ReCo: automated NGS read-counting of single and combinatorial CRISPR gRNAs. Bioinformatics (Oxford, England). 2023;39(8).
27. Gao Y, Zhao F. Computational Strategies for Exploring Circular RNAs. Trends in genetics : TIG. 2018;34(5):389-400.
28. Xiong Y, Chen X, Yang X, Zhang H, Li X, Wang Z, Feng S, Wen W, Xiong X. miRNA transcriptomics analysis shows miR-483-5p and miR-503-5p targeted miRNA in extracellular vesicles from severe acute pancreatitis-associated lung injury patients. Int Immunopharmacol. 2023;125(Pt A):111075.
29. Lim SH, Shin JH, Lee JW, Lee Y, Seo JH. Differences in the eyelid and buccal microbiome of glaucoma patients receiving long-term

administration of prostaglandin analog drops. Graefes Arch Clin Exp Ophthalmol. 2021;259(10):3055–65.
30. Montero O, Hedeland M, Balgoma D. Trials and tribulations of statistical significance in biochemistry and omics. Trends Biochem Sci. 2023;48(6):503–12.
31. Xiao H, Zou Y, Wang J, Wan S. A Review for Artificial Intelligence Based Protein Subcellular Localization. Biomolecules. 2024;14(4):409.
32. Tao Y, Luo R, Xiang Y, Lei M, Peng X, Hu Y. Use of bailing capsules (cordyceps sinensis) in the treatment of chronic kidney disease: a meta-analysis and network pharmacology. Front Pharmacol. 2024;15:1342831.
33. Liu X, Sun H, Zheng L, Zhang J, Su H, Li B, Wu Q, Liu Y, Xu Y, Song X, et al. Adipose-derived miRNAs as potential biomarkers for predicting adulthood obesity and its complications: A systematic review and bioinformatic analysis. Obesity reviews : an official journal of the International Association for the Study of Obesity. Obes Rev. 2024;25(7):e13748.
34. Huang R, Chen J, Dong X, Zhang X, Luo W. Transcriptome Data Revealed the circRNA-miRNA-mRNA Regulatory Network during the Proliferation and Differentiation of Myoblasts in Shitou Goose. Animals: an open access journal from MDPI. Animals (Basel). 2024;14(4):576.
35. Hao JJ, Liu Y, Lu JH, Zhao Y, Lin Y, Ma LQ, Xue P, Jin BY, Li BB, Zhou Z, et al. Analysis of the expression level and predictive value of CLEC16A|miR-654-5p|RARA regulatory axis in the peripheral blood of patients with ischemic stroke based on biosignature analysis. Front Neurol. 2024;15:1353275.
36. Kohansal M, Alghanimi YK, Banoon SR, Ghasemian A, Afkhami H, Daraei A, Wang Z, Nekouian N, Xie J, Deng X, et al. CircRNA-associated ceRNA regulatory networks as emerging mechanisms governing the development and biophysiopathology of epilepsy. CNS Neurosci Ther. 2024;30(4):e14735.
37. Chen A, Ji C, Li C, Brand-Saberi B, Zhang S. Multiple transcriptome analyses reveal mouse testis developmental dynamics. BMC Genomics. 2024;25(1):395.
38. Song W, Qiu J, Yin L, Hong X, Dai W, Tang D, Liu D, Dai Y. Integrated analysis of competing endogenous RNA networks in peripheral blood mononuclear cells of systemic lupus erythematosus. J Transl Med. 2021;19(1):362.
39. Mensah GA, Fuster V, Roth GA. Heart-Healthy and Stroke-Free World: Using Data to Inform Global Action. J Am Coll Cardiol. 2023;82(25):2343–9.
40. Wang Z, Yao M, Jiang L, Wang L, Yang Y, Wang Q, Qian X, Zhao Y, Qian J. Dexmedetomidine attenuates myocardial ischemia/reperfusion-induced ferroptosis via AMPK/GSK-3β/Nrf2 axis. Biomed Pharmacother. 2022;154:113572.
41. Li H, Yang DH, Zhang Y, Zheng F, Gao F, Sun J, Shi G. Geniposide suppresses NLRP3 inflammasomemediated pyroptosis via the AMPK signaling pathway to mitigate myocardial ischemia/reperfusion injury. Chin Med. 2022;17(1):73.
42. Du J, Li H, Song J, Wang T, Dong Y, Zhan A, Li Y, Liang G. AMPK Activation Alleviates Myocardial Ischemia-Reperfusion Injury by Regulating Drp1-Mediated Mitochondrial Dynamics. Front Pharmacol. 2022;13:862204.
43. Yin X, Guo Z, Song C. AMPK, a key molecule regulating aging-related myocardial ischemia-reperfusion injury. Mol Biol Rep. 2024;51(1):257.
44. Harrington JS, Ryter SW, Plataki M, Price DR, Choi AMK. Mitochondria in health, disease, and aging. Physiol Rev. 2023;103(4):2349–422.
45. Bharath LP, Agrawal M, McCambridge G, Nicholas DA, Hasturk H, Liu J, Jiang K, Liu R, Guo Z, Deeney J, et al. Metformin Enhances Autophagy and Normalizes Mitochondrial Function to Alleviate Aging-Associated Inflammation. Cell Metab. 2020;32(1):44-55.e6.
46. Tang Y, Xu W, Liu Y, Zhou J, Cui K, Chen Y. Autophagy protects mitochondrial health in heart failure. Heart Fail Rev. 2024;29(1):113–23.
47. Yi Q, Feng J, Lan W, Shi H, Sun W, Sun W. CircRNA and lncRNA-encoded peptide in diseases, an update review. Mol Cancer. 2024;23(1):214.
48. Ferreira HJ, Stevenson BJ, Pak H, Yu F, Almeida Oliveira J, Huber F, Taillandier-Coindard M, Michaux J, Ricart-Altimiras E, Kraemer AI, et al. Immunopeptidomics-based identification of naturally presented non-canonical circRNA-derived peptides. Nat Commun. 2024;15(1):2357.
49. Yang L, Wilusz JE, Chen LL. Biogenesis and Regulatory Roles of Circular RNAs. Ann Rev Cell Dev Biol. 2022;38:263-89.
50. Aufiero S, Reckman YJ, Pinto YM, Creemers EE. Circular RNAs open a new chapter in cardiovascular biology. Nat Rev Cardiol. 2019;16(8):503-14.
51. Kuznetsova I, Rackham O, Filipovska A. Investigating Mitochondrial Transcriptomes and RNA Processing Using Circular RNA Sequencing. Methods in molecular biology (Clifton, NJ). 2021;2192:43-57.
52. Zhao Q, Liu J, Deng H, Ma R, Liao JY, Liang H, Hu J, Li J, Guo Z, Cai J, et al. Targeting Mitochondria-Located circRNA SCAR Alleviates NASH via Reducing mROS Output. Cell. 2020;183(1):76-93.e22.
53. Cai L, Qi B, Wu X, Peng S, Zhou G, Wei Y, Xu J, Chen S, Liu S. Circular RNA Ttc3 regulates cardiac function after myocardial infarction by sponging miR-15b. J Mol Cellular Cardiol. 2019;130:10-22.
54. Guo J, Zhou Y, Cheng Y, Fang W, Hu G, Wei J, Lin Y, Man Y, Guo L, Sun M, et al. Metformin-Induced Changes of the Coding Transcriptome and Non-Coding RNAs in the Livers of Non-Alcoholic Fatty Liver Disease Mice. Cellular physiology and biochemistry : international journal of experimental cellular physiology, biochemistry, and pharmacology. 2018;45(4):1487-505.
55. Wang K, Gan TY, Li N, Liu CY, Zhou LY, Gao JN, Chen C, Yan KW, Ponnusamy M, Zhang YH, et al. Circular RNA mediates cardiomyocyte death via miRNA-dependent upregulation of MTP18 expression. Cell death and differentiation. 2017;24(6):1111-20.
56. Yu L, Wang Q, Liu N, Zhao J, Yu J, Tao S. Circular RNA circ-Ttc3 protects HaCaT cells from hypoxic injury by downregulation of miR-449a. IUBMB life. 2020;72(3):505-14.
57. Wang S, Li L, Deng W, Jiang M. CircRNA MFACR Is Upregulated in Myocardial Infarction and Downregulates miR-125b to Promote Cardiomyocyte Apoptosis Induced by Hypoxia. J Cardiovasc Pharmacol. 2021;78(6):802-08.
58. Jin X, Gao J, Zheng R, Yu M, Ren Y, Yan T, Huang Y, Li Y. Antagonizing circRNA_002581-miR-122-CPEB1 axis alleviates NASH through restoring PTEN-AMPK-mTOR pathway regulated autophagy. Cell death disease. 2020;11(2):123.
59. Li J, Wang X, Shi L, Liu B, Sheng Z, Chang S, Cai X, Shan G. A Mammalian Conserved Circular RNA CircLARP1B Regulates Hepatocellular Carcinoma Metastasis and Lipid Metabolism. Advanced science (Weinheim, Baden-Wurttemberg, Germany). 2024;11(2):e2305902.
60. Li Q, Yao H, Wang Y, Wu Y, Thorne RF, Zhu Y, Wu M, Liu L. circPRKAA1 activates a Ku80/Ku70/SREBP-1 axis driving de novo fatty acid synthesis in cancer cells. Cell reports. 2022;41(8):111707.
61. Kao WC, Chen JC, Liu PC, Lu CC, Lin SY, Chuang SC, Wu SC, Chang LH, Lee MJ, Yang CD, et al: The Role of Autophagy in Osteoarthritic Cartilage. Biomolecules. 2022;12(10).
62. Gong Z, Wang K, Chen J, Zhu J, Feng Z, Song C, Zhang Z, Wang H, Fan S, Shen S, et al. CircZSWIM6 mediates dysregulation of ECM and energy homeostasis in ageing chondrocytes through RPS14 posttranslational modification. Clin Translational Med. 2023;13(1):e1158.
63. LaFoya B, Prehoda KE. Actin-dependent membrane polarization reveals the mechanical nature of the neuroblast polarity cycle. Cell reports. 2021;35(7):109146.
64. Tzortzopoulos A, Thomaidou D, Gaitanou M, Matsas R, Skoulakis E. Expression of Mammalian BM88/CEND1 in Drosophila Affects Nervous System Development by Interfering with Precursor Cell Formation. Neurosci Bull. 2019;35(6):979–95.
65. Wolujewicz P, Steele JW, Kaltschmidt JA, Finnell RH, Ross ME. Unraveling the complex genetics of neural tube defects: From biological models to human genomics and back. Genesis. 2021;59(11):e23459.
66. Liu Y, Ouyang L, Mao C, Chen Y, Li T, Liu N, Wang Z, Lai W, Zhou Y, Cao Y, et al. PCDHB14 promotes ferroptosis and is a novel tumor suppressor in hepatocellular carcinoma. Oncogene. 2022;41(27):3570–83.
67. López-Varea A, Vega-Cuesta P, Ruiz-Gómez A, Ostalé CM, Molnar C, Hevia CF, Martín M, Organista MF, de Celis J, Culí J, et al. Genome-wide phenotypic RNAi screen in the Drosophila wing: phenotypic description of functional classes. G3 (Bethesda, Md). 2021;11(12).

Publisher's Note